# Combining circuit theory and numerical field calculations in designing mini-mechatronic systems

R.Belmans
Dept.Electrical Engineering-ESAT, Division Electrical Energy
K.U.Leuven
Belgium

K.Hameyer

**Abstract**—**In mechatronic system design, electrical motor are generally treated by a lumped parameter model and a torque versus speed or versus position characteristic. In the design and optimisation of electrical machines and actuators, as generally used for powering such mechatronics systems, modern finite element based CAD methods are employed. In order to link both approaches, macroscopic parameters are deducted from the microscopic field solution via the appropriate post-processing methods. For normal sized motors, this is a well known approach. However, for mini- and micromotors, requiring a three dimensional field solution, this is far less evident. Therefore, in this paper a technique is described to derive the parameters and the torques from the magnetic field for the magnetostatic motors and the electric field for electrostatic motors. The inductances, resp. capacitances are calculated. For the torque not only the average component, but also the torque variations as a function of the position are discussed.**

## INTRODUCTION

In modern systems, the trend is towards small packages, low power consumption, high efficiency and low cost. Consequently, the required drives need to have a small rotor inertia and volume. In a number of applications the disc-type motor is the best choice because of its short axial length. Also for portable devices, where the energy is supplied by a battery, there is crucial demand for a drive system with a high efficiency. To attain these goals, permanent magnets are used for the excitation and an electronic commutation can be combined with speed control.

As permanent magnet material, Nd-Fe-B has recently become very attractive. It shows the highest energy density of all commercially available materials. It provides high air gap flux density and makes a highly dynamic motor design feasible. To be able to make the best possible use of the material, the design has to be optimised using numerical field analysis techniques.

## MAGNETIC MINI-MOTOR

The main design features of the motor are:

- armature winding in the stator;
- rotor consists of a thin disc made of sintered multipole permanent magnet material;
- detection of rotor position by magneto resistive sensors.

Brushless axial field motors can be built up using a symmetrical or asymmetrical layout [1,2]. The prototype design is characterised by symmetrical planar windings, produced using etching techniques. The required torque makes it necessary to employ a multilayer winding to establish a sufficiently high current layer. The prototype features two phases on the stator and eight poles on the rotor. The rotor is a disc-type permanent magnet, magnetised in the axial direction. The stator consists of two disks of ferromagnetic back iron material with two airgap windings. On each stator side, 8 windings are installed and connected forming two phases. Each winding consists of four layers. In the second stator disk, the opposite connections are made to balance the electrical system. Geometrically, both stator parts are identical. However they are rotated with respect to each other. This unsymmetrical winding arrangement reduces the axial forces on the machine bearings. The outer diameter is about 45 mm and the axial length about 15 mm.

## MAIN CHARACTERISTICS

### *Field solution*

Because of its special geometry, this type of motor can not be analysed using a two dimensional approach, as generally found in modern design procedures [3]. Therefore, a three dimensional analysis is used [4,5]. The first finite element simulation is performed with the windings not carrying current. In the second finite element solution, the flux density distribution is obtained accounting for the combined action of permanent magnets and current carrying coils. The magnetic disc of the rotor is divided into 20 segments of 4.5°. When defining a magnetic problem using this model, all segments are assigned a material characteristic representing Nd-Fe-B. Ten segments are defined as a north pole, and ten as a south pole. By changing the north and south orientation of the labels when defining the next problem, a simulation of the stepwise rotation of the rotor is obtained. The calculation of the motor characteristics as a function of the rotor position is done without having to produce another

material mesh, leading to an important reduction of the computing time.

*Flux linkage, inducted voltage and inductance*

The flux $\Psi_w$ produced by the magnets and coupled with one winding, not carrying current, is calculated by integrating the flux density. By a stepwise rotor motion, $\Psi_w$ as a discrete function of the rotor position $\theta$ is obtained.

Using the discrete Fourier transform (DFT), the linked flux $\Psi_w$ can be expressed as a continuous function of $\theta$ and differentiated with respect to $\theta$. This derivative is used to calculate the induced voltage in one phase formed by four windings in series:

$$_{in-p} = -4\frac{d\Psi_w}{d\theta}\cdot\frac{n.2\pi}{60} \qquad (1)$$

where n is the constant rotating speed in rpm. This is an important macroscopic characteristic, since it can be compared with measured values. The result is a sine function with an amplitude of 0.55 V. The measured amplitude is 0.62 V at 1000 rpm.

The inductance of one phase (4 windings) is:

$$L = \left(\frac{4}{i}\right)(\Psi_{w,i} - \Psi_{w,0A}) = 14\ \mu H \qquad (2)$$

The current i in the phase is typically 0.5 A. $\Psi_{w,i}$ is the flux linked with the winding due to the current and the permanent magnets. $\Psi_{w,0A}$ is the flux linkage produced by the magnets alone. The measured value is 11.8 µH and thus lower. Several elements contribute to this discrepancy.

- In the real motor, the back iron is laminated; being impossible to model correctly, yielding a smaller reluctance and thus a larger inductance.
- In the model $\Psi_{phase} = 4\,\Psi_w$. In the real motor $\Psi_{phase} < 4\,\Psi_w$, because one of the 4 windings is smaller to provide space for the position sensor.
- The coil is represented by a band winding and does not match the material mesh outline.

*Torque Calculation*

Three methods yield the torque. The first one uses the interaction between current and flux density. The force per unit volume on current-carrying conductors is integrated along the conductor and the contributions of the different conductors are added. The second one is based on the virtual work: The torque is given by derivative of the co-energy with respect to the rotor position. The third method is the integration of the Maxwell stress tensor on a surface surrounding the rotor also yields the torque.

Using the interaction between current and flux density, the motor torque developed on the rotor when one coil is active, is calculated as a function of the rotor position (Fig.1). Applying a discrete Fourier transform the fundamental component is found:

$$T = -2.466\sin(4\theta) \quad [mNm] \qquad (3)$$

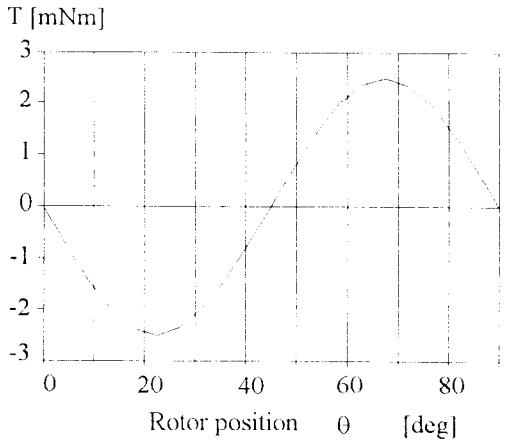


Fig.1. Torque obtained from current - field interaction (First winding supplied with 0.5 A)

Using the virtual work method, care has to be taken to obtain sufficient accuracy. Again a DFT has to be used to find the fundamental component. This method suffers from the need to differentiate the stored energy, leading to numerical inaccuracies. A sufficient number of models has to be used that are close enough to allow the differentiation with respect to the angle. This is a drawback of this method when compared to the method of current-field interaction. However, if the torque as a function of the rotor position is to be found, several models are required anyway, and the drawback is not longer important. The result of the virtual work method is $4*(4A_1) = 2.544$ mNm. This value matches well the result obtained in the current-field interaction method.

The Maxwell stress tensor has to be evaluated on a surface enclosing the rotor. This yields a lot of numerical problems as it requires projections of the flux density distribution and several differentiations, reducing the accuracy of the results. Therefore, the Maxwell stress tensor is generally not used for torque calculations.

Due to the low values for the torque as found in minimotors, the solutions for the different windings may be found by superposition. Figure 2 shows the 4 torque curves resulting from operating the 4 coils over one

period. The basic curve is the torque $T_1$ obtained from the current - field interaction method (figure 1). The other 3 are calculated from $T_1$ by shifting the curves in time:

$$T_2(\theta) = T_1(\theta + 45°)$$
$$T_3(\theta) = T_1(\theta + 22.5°) \quad (4)$$
$$T_4(\theta) = T_1(\theta + 67.5°)$$

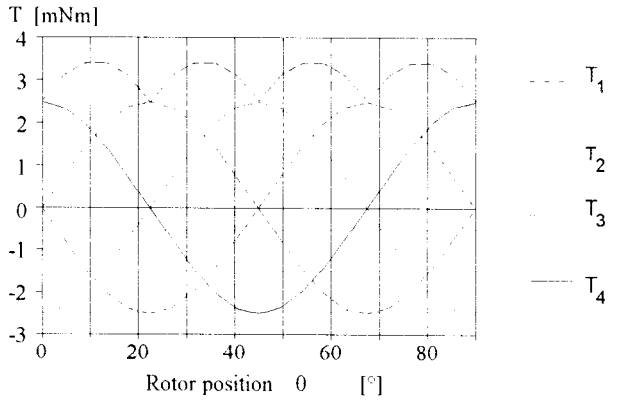


Fig.2. Torque curves for the disc-type motor (Windings supplied with 0.5 A)

Fig. 2 also gives the resulting torque when switching is done for a counter-clock-wise rotation. This means that only the coils giving a positive torque are active. In this 4 coil configuration it means that at every position, 2 coils are active: one in the top, one in the bottom stator. The properties of the sum torque are:

- periodicity of 22.5° (1/4 of motor periodicity);
- average torque 3.14 mNm;
- peak to peak ripple 1.02 mNm.

## ELECTROSTATIC MICROMOTORS

The same type of approach as discussed with the magnetic minimotors is used for electrostatic motors. Here, the torque production is based on the variation of the capacitance between the rotor and the stator as they move relative to each other. In practice two types of motor geometries are used. The first one has an radial electric field (fig.3). Here the value of the torque highly depends on the rotor length, which therefore has to be high compared to the diameter. Such a design requires the use of the very expensive LIGA technology [6]. When dealing with motors with an axial electric field, more common etching techniques may be used, yielding a far less expensive manufacturing process [7]. However, both designs require a 3D solution of the electric field in order to obtain sufficiently accurate results for both the field itself and the macroscopic parameters that may be deducted from it. The results in this paper deal with the LIGA type of motor. However, the same approach can be used for the axial field type of motor.

Building 3D meshes is time consuming. Therefore performing optimisation in 3D is very tedious since a large number of models, slightly different from one another, must be built and analysed. For micromotor structures the required labour is even vaster since for every model the analysis normally must be carried out for a number of rotor positions, in order to obtain macroscopic parameters as torque and capacitance as function of the rotor position. Therefore, software techniques are developed in order to construct automatically the 3D meshes yielding structures to optimise the design with the objective to average torque or torque ripple [8]. The excitation voltage are applied as boundary conditions to the model. Currents are not present in the electrostatic model, nor are charges. After the electric field is solved, the postprocessor is used to evaluate the macroscopic parameters.

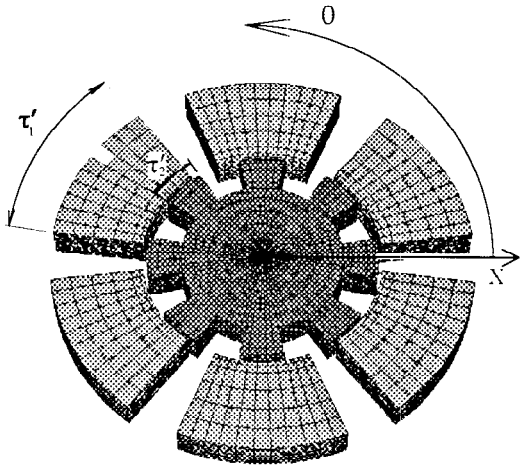


Fig. 3. 3D mesh of a 6/8 pole electrostatic radial flux micromotor

## EQUIVALENT CIRCUIT MODEL

The information gained from two different excitations as a function of the rotor positions is sufficient to create an equivalent circuit describing the motor geometry. The circuit used for a 6/8 pole motor (fig.4) consists of 12 capacitors, twice the number of stator poles. The capacitances vary with the rotor position. Writing $C_k^{SR}(\alpha)$ for the capacitance between stator electrode $k$ and the rotor, C1 to C6, and $C_k^{SS}(\alpha)$ for the capacitance between stator electrode $k$ and the next stator electrode, C7 to C12, it can be seen that the difference between capacitances with different index $k$ is only a phase shift equal to a multiple of the stator pole pitch. With two different excitations for n rotor positions, the stored energy, obtained from the field solution, is calculated and a set of equations is solved yielding $C_k^{SR}(\alpha)$ and $C_k^{SS}(\alpha)$. The

torque is calculated using an analytical differentiation (virtual work). To the equivalent circuit any kind of excitation can be applied. The block-wave is the most common, since it is the most powerful. To minimise radial forces, the motor is excited symmetrically (Fig.5). Applying these excitations to the equivalent circuit the torque as a function of the rotor position is calculated (Fig.6). By switching from one excitation to another at the crossovers marked by arrows, the optimum excitation is achieved. The average torque is found by integrating the curve following the highest torque. The torque ripple may be deducted.

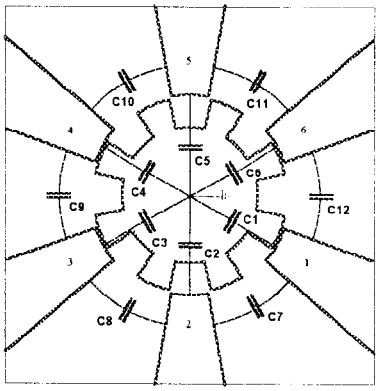


Fig.4. Equivalent circuit for an electrostatic motor with 6 stator poles

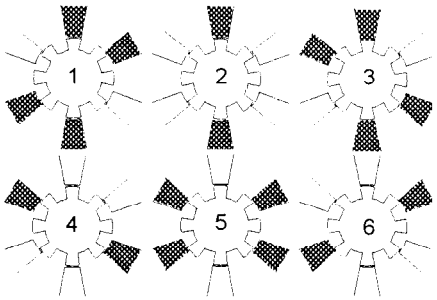


Fig.5. Possible symmetric excitations of a motor with six electrodes

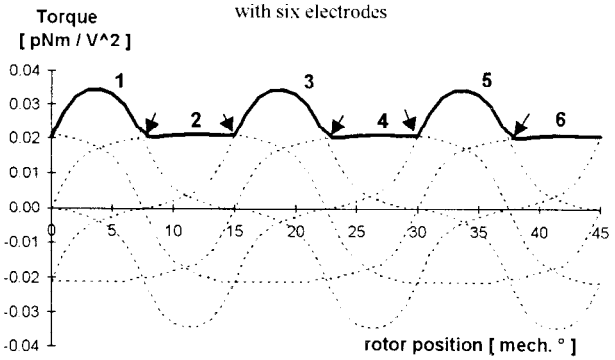


Fig.6. Torque vs. rotor position for 6 different excitations (6/8 pole motor)

## Conclusions

Using advanced 3D field solutions, the geometry of both magnetic minimotors and electrostatic micromotors can be optimised. However, the results of this optimisation procedure is not directly useful for mechatronic system design. Therefore, it was shown how the field solution may be linked with the equivalent circuit, via the inductances of the magnetic motor and the capacitances of the electrostatic machine. Apart from these parameters, the torque characteristic of both systems may be found. Not only the average torque is calculated, but also the torque ripple has been taken into account also. Using such an approach, even special excitation methods may be found, leading to a maximisation of the torque output for a given geometry. Such a technique allows rapid software prototyping of mechatronic systems, increasing tremendously the flexibility, that is not achievable using classic prototyping. The number of prototypes and designs is virtually unlimited, certainly if automated shells are built to construct the finite element meshes and to postprocess the results in order to obtain the macroscopic parameters required in the system simulation.

## Acknowledgements

The authors are grateful to the Commission of the European Communities for funding the work within the BRITE-EuRAM framework, project no.BE-3360. The authors are indebted to the Belgian Nationaal Fonds voor Wetenschappelijk Onderzoek for its financial support for this work and the Belgian Ministry of Scientific Research for granting the project IUAP No. 51 on Magnetic Fields.

## References

[1] C.-S.Park: "Theoretische und experimentelle Untersuchungen an einem elektronisch kommutierten Scheibenläufer-Kleinmotor", Ph.D. Thesis, T.U. Berlin, 1989.

[2] R.Hanitsch, C.S..Park: "Performance of a sub fractional HP disc-type motor", ICEM'90, 13-15.8.1990, MIT, Cambridge USA, Vol. 1, pp. 138 - 142.

[3] D.A.Lowther, P.P.Silvester: "Computer-Aided Design in Magnetics", Springer-Verlag, Berlin Heidelberg New-York, 1985.

[4] R.Belmans, D.Verdyck, M.Van Dessel, W.Geysen, R.Hanitsch, E.S. Hemead: "Three dimensional finite element analysis in axial flux permanent magnet motors," Proc.Speedam, Positano(It.) May 19-21, 1992

[5] St.Henneberger, M.Van Dessel, R.Belmans, R.Hanitsch: "Design of a small brushless disc-type motor with permanent using 3D finite elements." ICEM 1994, Paris, France, 5-8 Sept. 1994, Vol..1, pp.148-153.

[6] J.Mohr, C.Burham, P.Bley, W Menz, U.Wallrabe: "Movable microstructures manufactured by the LIGA process as basic elements for microsystems," In H.Reichl (editor). Micro systems Technologies 90, Springer Verlag, pp.529-537 (1990).

[7] H.Ziad, S.Spirkovitch, S.Rigo: "MMIC applications for electrostatic motors," Proc. of the Actuator 94 Conference, Bremen, June 1994.

[8] T.B.Johansson, M.Van Dessel, R.Belmans, W.Geysen: "Technique for finding the optimum geometry of electrostatic micromotors," IEEE Transactions on Industry Applications, Vol.30, No.4, July/August 1994, pp.912-919.